SCIENTIFIC REPORTS

OPEN

A Fluctuating State in the Framework Compounds $(Ba,Sr)Al_2O_4$

Received: 23 July 2015
Accepted: 27 November 2015
Published: 13 January 2016

Yui Ishii, Hirofumi Tsukasaki, Eri Tanaka & Shigeo Mori

The structural fluctuation in hexagonal $Ba_{1-x}Sr_xAl_2O_4$ with a corner-sharing AlO_4 tetrahedral network was characterized at various temperatures using transmission electron microscopy experiments. For $x \leq 0.05$, soft modes of q ~ (1/2, 1/2, 0) and equivalent wave vectors condense at a transition temperature (T_C) and form a superstructure with a cell volume of $2a \times 2b \times c$. However, T_C is largely suppressed by Sr-substitution, and disappears for $x \geq 0.1$. Furthermore, the q ~ (1/2, 1/2, 0) soft mode deviates from the commensurate value as temperature decreases and survives in nanoscaled regions below ~200 K. These results strongly suggest the presence of a new quantum criticality induced by the soft mode. Two distinct soft modes were observed as honeycomb-type diffuse scatterings in the high-temperature region up to 800 K. This intrinsic structural instability is a unique characteristic of the framework compound and is responsible for this unusually fluctuating state.

Novel phases near the ordered states of spins, charges, or orbitals of electrons have long been fascinating subjects in condensed matter physics. Notable examples are superconductivity near an antiferromagnetic order, a charge density wave (CDW), a spin density wave (SDW), and an orbital order, which are typically found in cuprates, transition metal dichalcogenides[1], iron arsenides[2], and ruthenates[3]. The accumulated knowledge from these studies has provided us with the simple and universal description that an extraordinary state often emerges from the fluctuation in an ordered state of the spins, charges, or orbitals. Just as an electron, a phonon is a fundamental quantum in a crystal. Despite a large number of experimental and theoretical studies that focus on fluctuations in these three aspects of electrons, there are few studies on the new phenomenon in which the "fluctuation in phonons" plays a key role.

In framework compounds containing linked polyhedra, for example, several modifications of silicates[4,5], nepheline[6], and ZrW_2O_8[7], the existence of correlated motions of polyhedra within the network structure has been reported. These correlated motions are called "rigid unit modes" (RUMs)[8–10]. These RUMs sometimes act as a soft mode that induces a structural phase transition, for example, the structural phase transitions in quartz[4], tridymite[5], and nepheline[6]. For the framework compound $BaAl_2O_4$, it has also been argued that a RUM is the dominant structural instability[11].

$BaAl_2O_4$ crystallizes in a staffed tridymite-type crystal structure[12–15] that comprises a three-dimensional network of corner-sharing AlO_4 tetrahedra with six-membered cavities of the tetrahedral network occupied by alkaline earth ions. In the electron diffraction patterns of its high-temperature phase, characteristic honeycomb-like diffuse scatterings (honeycomb pattern) have been observed[16]. Because the scattering intensities are strongly dependent on the temperature, the characteristic honeycomb pattern may stem from an intrinsic structural fluctuation associated with a soft mode. A recent study of the structural phase transition using synchrotron X-ray diffraction revealed that this system possesses two types of soft modes both of which give rise to strong diffuse scattering intensities which sharply increase towards the structural phase transition temperature (T_C), indicating that both modes condensed simultaneously at T_C[17]. In addition, this compound exhibits an improper ferroelectricity that is accompanied by the structural phase transition at approximately 400 K[12,13,18]. This transition temperature has been reported to decrease rapidly via the *AE*-site disorder, such as the partial substitution of Sr for Ba[19]. Motivated by the analogy of the fluctuation in the ordered state of spins, charges, or orbitals, we investigated the structural fluctuation in the *AE*-site disordered $BaAl_2O_4$.

In the present study, both the temperature variation of the diffuse scatterings and the structural phase transition temperature for $Ba_{1-x}Sr_xAl_2O_4$ are systematically studied by transmission electron microscopy (TEM). We

Department of Materials Science, Osaka Prefecture University, Sakai, Osaka 599-8531, Japan. Correspondence and requests for materials should be addressed to Y.I. (email: ishii@mtr.osakafu-u.ac.jp)

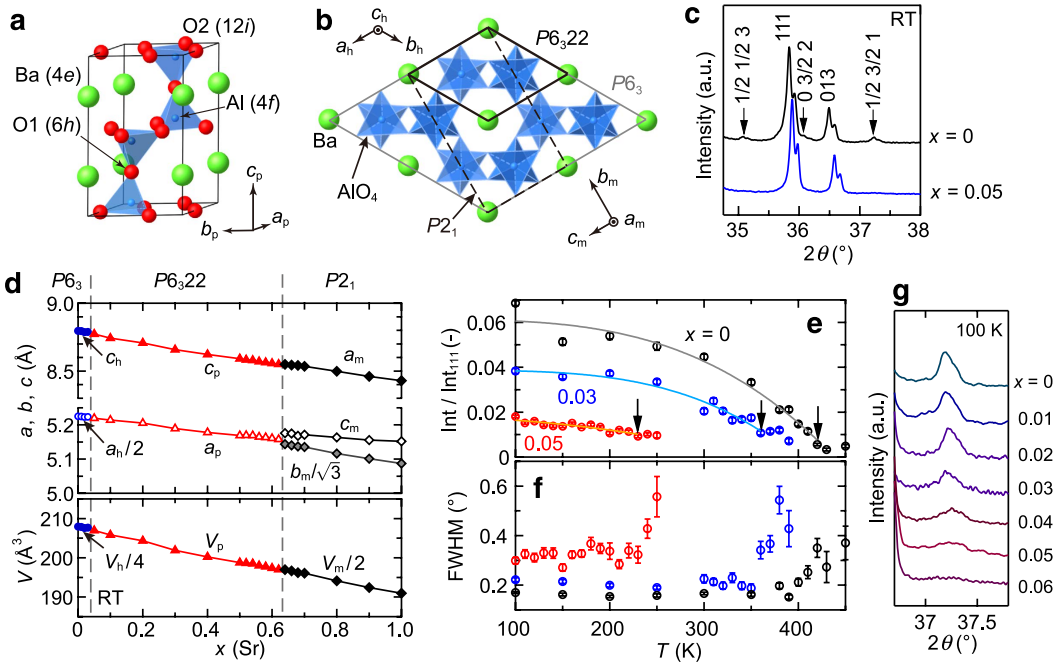

Figure 1. Structural change in $Ba_{1-x}Sr_xAl_2O_4$. (**a**) Hexagonal $P6_322$ parent crystal structure of $BaAl_2O_4$. (**b**) Various cell settings for $BaAl_2O_4$ and $SrAl_2O_4$. The thick solid line and grey line represent the unit cell of the $P6_322$ parent structure and the $P6_3$ low temperature phase of $BaAl_2O_4$, respectively. The broken line shows the $P2_1$ low temperature phase of $SrAl_2O_4$, which has the same crystal structure as $BaAl_2O_4$ at high temperature. (**c**) Powder XRD profiles in the range of $2\theta = 35$–$38°$ for $Ba_{1-x}Sr_xAl_2O_4$ ($x = 0$ and 0.05) polycrystalline samples at room temperature. The superlattice reflections are observed in the $x = 0$ sample, as indicated by the arrows. (**d**) Variation of the lattice parameters at room temperature plotted against the nominal Sr-substitution level x. The circle, triangle, and diamond symbols represent the lattice parameters of the $P6_3$, $P6_322$, and $P2_1$ crystal structures, respectively. (**e**) Temperature dependence of the intensity of the 1/2 3/2 1 superlattice reflection normalized by the intensity of the 111 fundamental reflection. Solid lines are fitted curves to show the trend. The error bars are the standard deviations. The arrows indicate the T_C values. (**f**) FWHM as a function of temperature. (**g**) Powder XRD profiles near the 1/2 3/2 1 superlattice reflection of $Ba_{1-x}Sr_xAl_2O_4$ with $x = 0$–0.06 obtained at 100 K.

report an unusual state lying below 200 K for $Ba_{1-x}Sr_xAl_2O_4$ with $x \geq 0.1$ in which the dynamic structural fluctuation develops as the temperature decreases.

Results and Discussion

The high-temperature phase of $AEAl_2O_4$ (AE = Sr or Ba) crystallizes into a hexagonal structure with the space group $P6_322$, as shown in Fig. 1a. The low-temperature ferroelectric phase of $BaAl_2O_4$ below T_C has been identified as a hexagonal $P6_3$ superstructure with $a_h = 2a_p$, $b_h = 2b_p$ and $c_h = c_p$, where the subscripts h and p denote the hexagonal low-temperature structure and the high-temperature parent structure, respectively. $SrAl_2O_4$ crystallizes into the $P2_1$ monoclinic structure below 950 K[15]. The cell settings of $P6_322$, $P6_3$, and $P2_1$ are shown in Fig. 1b. The subscript m denotes the $P2_1$ monoclinic structure. Figure 1c shows the powder X-ray diffraction (XRD) profiles of $Ba_{1-x}Sr_xAl_2O_4$ ($x = 0$ and 0.05) in the range of $2\theta = 35$–$38°$ at room temperature. The superlattice reflections of $P6_3$ low-temperature phase, which are marked by arrows, are clearly observed for $x = 0$, whereas they cannot be observed for $x = 0.05$. This indicates that $x = 0$ sample crystallizes in the $P6_3$ crystal structure at room temperature while $x = 0.05$ sample has the $P6_322$ symmetry. High-resolution TEM (HRTEM) experiments for $x = 0$ sample also revealed that the fine antiphase domains with $P6_3$ symmetry cover the entire area of the crystal, as shown in Supplementary Fig. S1 online. The samples with $0.05 \leq x \leq 0.62$ crystallize in the $P6_322$ parent structure at room temperature. Figure 1d shows the lattice parameters at room temperature plotted against the nominal Sr content x. A linear decrease in these parameters as x increases indicates a systematic substitution of Sr with a smaller ionic radius than Ba. The $P2_1$ monoclinic structure appears above $x = 0.64$. Thus, we focus on the structural phase transition from $P6_322$ to $P6_3$ for samples with $x < 0.6$.

Figure 1e,f represent the 1/2 3/2 1 superlattice intensities and the full width at half maximums (FWHMs) for $x = 0$, 0.03, and 0.05 samples, respectively, as a function of temperature. The data were obtained during heating. The superlattice intensities are normalized using the intensities of the 111 fundamental reflections (Int_{111}). For $x = 0$, the structural phase transition occurs at 420 K, with an abrupt decrease in the superlattice intensity and simultaneous increase in the FWHM. The transition temperature decreases as x increases, which is consistent with a previous report[19]. Figure 1g shows the 1/2 3/2 1 superlattice intensities for $x = 0$–0.06 at 100 K. The

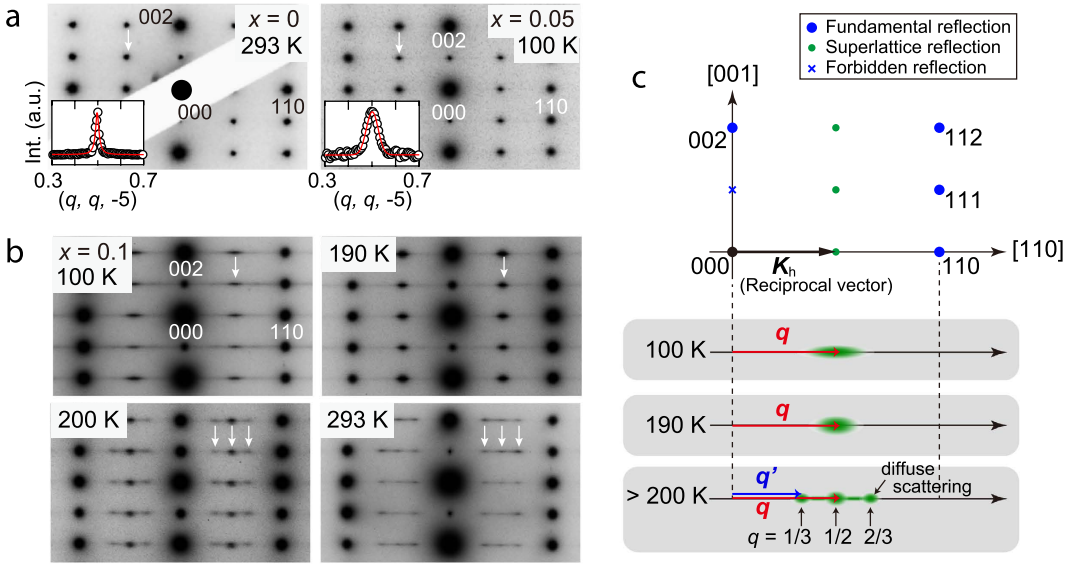

Figure 2. Diffuse scatterings of $Ba_{1-x}Sr_xAl_2O_4$. (**a**) Diffraction patterns for $x = 0$ single crystal at 293 K (left) and $x = 0.05$ polycrystalline sample at 100 K (right) obtained with a $[\bar{1}10]$ incidence. Forbidden reflections with $00l$ ($l = 2n + 1$) are observed because of multiple reflections. The insets show the line scans of 1/2 1/2 $\bar{5}$ superlattice reflections along [110]. (**b**) Temperature variation of the diffraction patterns with a $[\bar{1}10]$ incidence for $x = 0.1$. The arrows indicate the diffuse scatterings. (**c**) Schematic drawings of the relation between a reciprocal vector $\boldsymbol{K}_h$ and the wave vectors $\boldsymbol{q} \sim (1/2, 1/2, 0)$ and $\boldsymbol{q}' \sim (1/3, 1/3, 0)$.

superlattice intensity decreases and the FWHM increases as x increases, as shown in Fig. 1g. This result indicates that the correlation length of the superstructure decreases with increasing the Sr-concentration x. For $x = 0.06$, weak intensities of 1/2 3/2 1 resulted in broad peaks even though they were largely independent of temperature. Discontinuities in the lattice parameters could not be detected at the T_C for each composition.

To investigate the structural fluctuation in the $Ba_{1-x}Sr_xAl_2O_4$, electron diffraction experiments were performed between 100 and 800 K during heating. Figure 2a shows the $[\bar{1}10]$-zone axis electron diffraction patterns obtained for $x = 0$ at 293 K (left panel) and $x = 0.05$ at 100 K (right panel). The superlattice reflections at the $h + 1/2\ k + 1/2\ l$ reciprocal positions, marked by arrows in Fig. 2a, indicate the $P6_3$ superstructure. However, the superlattice reflections for $x = 0.05$ are broader than that for $x = 0$; these reflections for $x = 0.05$ are slightly elongated in the [110] direction. The 1/2 1/2 $\bar{5}$ superlattice reflections for $x = 0$ and 0.05 are scanned along [110] in the insets. The FWHM for the superlattice reflection of $x = 0.05$ is clearly larger than that of $x = 0$. Surprisingly, the diffuse scattering appears around the superlattice reflections for $x = 0$ at 310 K, as shown in Supplementary Fig. S2 online, which is 110 K lower than the T_C. Above the T_C, two distinct diffuse scatterings near the $h + 1/2\ k + 1/2\ l$ and $h + 1/3\ k + 1/3\ l$ reciprocal positions are observed, as well as diffuse streaks in between them (see Supplementary Figs. S2 and S3 online). Recently synchrotron X-ray diffraction experiments and the first principles calculations have revealed that these diffuse scatterings are ascribed to $\boldsymbol{q} \sim (1/2, 1/2, 0)$ and $\boldsymbol{q}' \sim (1/3, 1/3, 0)$ soft modes[17]. That is, two distinct soft modes coexist above the T_C because of structural instabilities. To the best of our knowledge, this coexistence has not been reported in other compounds thus far.

By contrast, $Ba_{1-x}Sr_xAl_2O_4$ ($0.1 \leq x \leq 0.5$) exhibits an unusual state below ~ 200 K, in which a soft mode fluctuates in $\boldsymbol{k}$-space. In this state, the low-energy soft mode with the symmetrically equivalent three $\boldsymbol{q}$s, $\boldsymbol{q}_1 \sim (1/2, 1/2, 0)$, $\boldsymbol{q}_2 \sim (1, -1/2, 0)$ and $\boldsymbol{q}_3 \sim (-1/2, 1, 0)$ in the reciprocal space, deviate from the commensurate $\boldsymbol{q}$ as the temperature decreases. Figure 2b and Supplementary Fig. S4 online shows the temperature variation of the electron diffraction patterns for $x = 0.1$ obtained during heating from 100 K. Above 200 K, diffuse scatterings near the $h + 1/2\ k + 1/2\ l$ and the $h + 1/3\ k + 1/3\ l$ reciprocal positions appear. At 190 K, the diffuse scatterings near $h + 1/2\ k + 1/2\ l$ reciprocal positions still exist, as indicated by an arrow in the figure, while the diffuse scatterings near the $h + 1/3\ k + 1/3\ l$ reciprocal positions disappear. Furthermore, these diffuse scatterings change the shape as temperature decreases; they are significantly elongated at 100 K. This strongly indicates that the $\boldsymbol{q} \sim (1/2, 1/2, 0)$ soft mode does not condensate to form the $P6_3$ superstructure but survives as a fluctuating state. These changes are schematically shown in Fig. 2c. The significant elongation of the diffuse scattering along [110] implies the deviation of $\boldsymbol{q} \sim (1/2, 1/2, 0)$ wave vector from the commensurate wave vector. It was confirmed that these changes took place reversibly during a thermal cycle. Similar results were obtained for $x = 0.3$, 0.4, and 0.5.

The structure variation in $Ba_{1-x}Sr_xAl_2O_4$ is summarized in Fig. 3a together with [001]-zone axis electron diffraction patterns (Fig. 3b–e). The black solid line indicates the T_C determined from the XRD. The broken line for $x \leq 0.05$ corresponds to the T_s, below which the diffuse scatterings disappear. Diffuse scatterings near the $h + 1/2\ k + 1/2\ l$ and $h + 1/3\ k + 1/3\ l$ positions are observed for temperatures between T_C and T_s in addition to the superlattice reflections, as shown in Fig. 3b (see also Supplementary Figs. S2 and S3 online). T_f denotes the temperature below which the $\boldsymbol{q}$ vectors of the soft modes deviate from the commensurate value. The coexistence of the two types of diffuse scatterings, which gives rise to the characteristic honeycomb pattern, was observed for

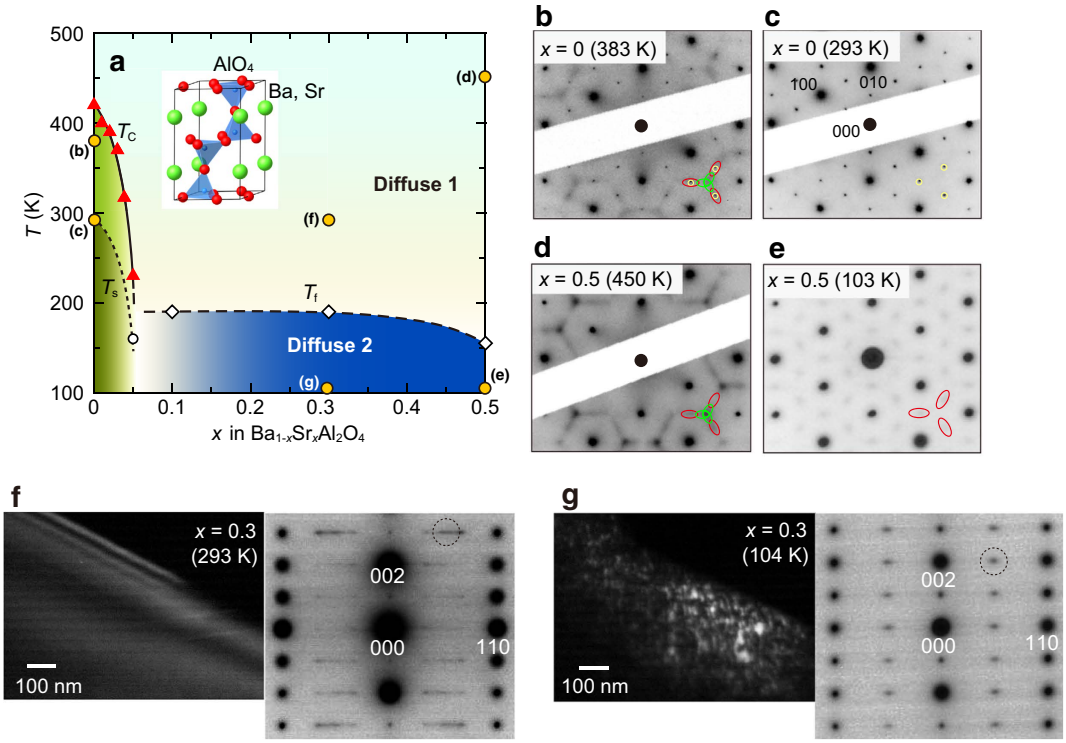

Figure 3. Summary of the results. (**a**) Structural phase diagram for $Ba_{1-x}Sr_xAl_2O_4$. The closed triangles correspond to the T_C determined from XRD experiments. T_s (open circle) for $x \leq 0.05$ and T_f (open diamonds) for $x \geq 0.1$ represent the temperatures below which the diffuse scatterings near the $h + 1/3\ k + 1/3\ l$ reciprocal positions disappear. (**b**–**e**) Typical electron diffraction patterns for each region. The superlattice reflections are marked by yellow circles in the electron diffraction patterns. In the region above T_C and T_f, which is denoted as "Diffuse 1", both the diffuse scatterings near the $h + 1/2\ k + 1/2\ l$ (red ellipsoids) and $h + 1/3\ k + 1/3\ l$ (green ellipsoids) reciprocal positions are observed, as well as the diffuse streaks in between them. In the region below T_f, which is denoted as "Diffuse 2", only the diffuse scatterings near $h + 1/2\ k + 1/2\ l$ are observed. (**f**,**g**) Dark-field TEM images, including the corresponding electron diffraction patterns at 293 and 104 K, respectively, for $x = 0.3$ using one of the $h + 1/2\ k + 1/2\ l$ diffuse scattering indicated by the dotted circle.

a wide temperature region above T_C and T_f for all compositions. For $x = 0.5$, this coexistence was observed even at 798 K, as shown in Supplementary Fig. S5 online. This region above T_C and T_f is denoted as "Diffuse 1" in Fig. 3a, and the region below T_f is denoted as "Diffuse 2".

To gain insight into the structural change at T_f, the microstructure observations were performed on $Ba_{1-x}Sr_xAl_2O_4$ with $x = 0.3$ using TEM. High-resolution TEM images at 293 K revealed homogeneous lattice fringes with no additional characteristic contrast, such as structural antiphase boundaries (see Supplementary Fig. S6 online). Moreover, fast Fourier transform calculations of the high-resolution TEM images reproduced the experimentally obtained electron diffraction pattern which includes two distinct diffuse scatterings near the $h + 1/2\ k + 1/2\ l$ and $h + 1/3\ k + 1/3\ l$ reciprocal positions and diffuse streaks in between them in addition to the fundamental reflections. Figure 3f,g show the dark-field TEM images and the corresponding electron diffraction patterns of the $x = 0.3$ sample obtained at 293 and 104 K, respectively, using one of the $h + 1/2\ k + 1/2\ l$ diffuse scatterings indicated by dotted circle in Fig. 3f,g under the two-beam condition. There is a homogeneous black region that covers the entire area at 293 K, as shown in Fig. 3f, indicating no superstructure in Diffuse 1 region. Alternating darker and brighter stripes observed in the wedge-shaped region is due to thickness fringes. However, island-like nanoscaled regions with ~20 nm in width are observed as black or white speckles at 104 K, as shown in Fig. 3g. Because the diffuse scatterings near $h + 1/2\ k + 1/2\ l$ reciprocal positions are strongly dependent on the temperature below ~200 K, it is reasonable to consider that the $\boldsymbol{q}$ ~ (1/2, 1/2, 0) soft mode still survives in each nanoscaled region.

Because the $\boldsymbol{q}$ ~ (1/2, 1/2, 0) soft mode does not condensate but instead fluctuate as the temperature decreases, no structural phase transition at lower temperature is expected. Such nanoscaled regions have been observed in several compounds[20–24]. For example, in $AlV_{2-x}Cr_xO_4$[20,21], the charge ordered state is suppressed by Cr doping and a spin-glass ground state appears. In $TiSe_2$[23] and Cu_xTiSe_2[24], it has been suggested that the onset of superconductivity is associated with the formation of domain walls in the CDW order[25]. Our results strongly suggest the presence of a quantum criticality that the structurally fluctuating state remains intact down to absolute zero temperature without a phase transition. Recently, structural quantum criticality has been discussed for the iron-arsenide superconductor $Ba(Fe_{1-x}Co_x)_2As_2$, in which the elastic constant softens in the vicinity of superconductivity[26]. Although $Ba_{1-x}Sr_xAl_2O_4$ is a good insulator, a small amount of nonstoichiometry in Ba and O has

been reported in this system[27]. Precise control of this nonstoichiometry is believed to open a path to develop new functional materials that possess a strong coupling of the conduction electrons with the structural fluctuation.

The large structural fluctuation in this compound can be attributed to the intrinsic structural instability caused by the RUMs[8–10] in the framework compounds with corner sharing polyhedra. These modes are well known in the modifications of SiO_2, e.g., α-quartz and β-tridymite, in which the RUMs act as the soft modes and induce the incommensurate phase transition or the successive phase transition[4,5]. In $BaGa_2O_4$ stuffed tridymite-type compound, the intrinsic structural instability is related to the mismatch between the average and interatomic distances[28]. In $Ba_{1-x}Sr_xAl_2O_4$, a slight change in the structural instability because of atoms occupying the hexagonal channels in a tridymite-type crystal structure would be responsible for the coexistence of the two distinct soft modes in the high-temperature region and for the emergence of the fluctuating low-temperature region dominated by the nanoscaled regions. To clarify the nature of these fluctuating states and the mechanism of the fluctuation in $Ba_{1-x}Sr_xAl_2O_4$, structural refinements using synchrotron XRD experiments down to the temperature of liquid He are now in progress.

In conclusion, we found that the ordered phase with $P6_3$ superstructure in $BaAl_2O_4$ is rapidly suppressed by the substitution of Sr for Ba. The unusually fluctuating state with $\boldsymbol{q} \sim (1/2, 1/2, 0)$ soft mode grows below 200 K in the compositional range between $x = 0.1$ and 0.5. Nanoscaled regions are dominant in this compositional window, indicating that no structural phase transition occurs to the ground state. The intrinsic structural instability in the AlO_4 tetrahedral network is responsible for this low-temperature fluctuating state.

Methods

Polycrystalline samples of $Ba_{1-x}Sr_xAl_2O_4$ ($0 \leq x \leq 1$) were synthesized using a conventional solid-state reaction. $BaCO_3$ (99.9%), $SrCO_3$ (99.9%), and Al_2O_3 (99.99%) powder were mixed at a molar ratio of 1:1 and calcined at 1200 °C for 10 h and at 1300 °C for 12 h in air with intermediate grinding. The obtained powder was pressed into a pellet, sintered at 1450 °C for 48 h, and then furnace cooled to room temperature. These pellets were stored in a vacuum. Single crystals of $BaAl_2O_4$ were prepared using a self-flux method in a platinum crucible. A mixture of previously synthesized $BaAl_2O_4$ and $BaCO_3$ with a molar ratio of 50:17 was heated at 1470 °C for 6 h and then slowly cooled to 1200 °C at a rate of 2 °C/h. After furnace cooling to room temperature, colourless transparent crystals with a hexagonal shape and with edges approximately 100 μm in length were mechanically separated from the flux. Samples obtained from the flux were stored in a vacuum. Powder XRD was performed using Cu-Kα radiation in a temperature range between 100 and 500 K. The powder XRD profiles revealed that all of the polycrystalline samples are single-phase samples. Single-crystal XRD experiments also revealed that the crystals have the $P6_3$ crystal structure at room temperature. *In situ* TEM observations were performed in a temperature range of 100 to 800 K using a double-tilted liquid N_2 cooling holder and heating holder in the JEM-2010 TEM system (JEOL, Japan). After the desired temperature was reached, all of the diffraction patterns were collected with a time interval of more than 30 min until no changes in the diffraction pattern were observed. All of the indices in the XRD profiles and the electron diffraction patterns are based on the $P6_322$ parent phase throughout this paper.

References

1. Rossnagel, K. On the origin of charge density waves in select layered transition-metal dichalcogenides. *J. Phys. Condens. Matter* **23,** 213001 (2011).
2. Canfield, P. C. & Bud'ko, S. L. FeAs-based superconductivity: a case study of the effects of transition metal doping on $BaFe_2As_2$. *Ann. Rev. Cond. Matter Phys*. **1,** 27–50 (2010).
3. Nakatsuji, S. & Maeno, Y. Quasi-two-dimensional Mott transition system $Ca_{2-x}Sr_xRuO_4$. *Phys. Rev. Lett.* **84,** 2666–2669 (2000).
4. Hammonds, K. D., Dove, M. T., Giddy, A. P., Heine, V. & Winkler, B. Rigid-unit phonon modes and structural phase transitions in framework silicates. *Am. Mineralogist* **81,** 1057–1079 (1996).
5. Pryde, A. K. A. & Dove, M. T. On the sequence of phase transitions in tridymite. *Phys. Chem. Minerals* **26,** 171–179 (1998).
6. Hayward, S. A., Pryde, A. K. A., de Dombal, R. F., Carpenter, M. A. & Dove, M. T. Rigid Unit Modes in disordered nepheline: a study of a displacive incommensurate phase transition. *Phys. Chem. Minerals* **27,** 285–290 (2000).
7. Tucker, M. G. *et al.* Negative Thermal Expansion in ZrW_2O_8: Mechanisms, Rigid Unit Modes, and Neutron Total Scattering. *Phys. Rev. Lett.* **95,** 255501 (2005).
8. Dove, M. T., Giddy, A. P. & Heine, V. Rigid unit mode model of displacive phase transitions in framework silicates. *Trans. Am. Cryst. Assoc*. **27,** 65–75 (1991).
9. Dove, M. T., Giddy, A. P. & Heine, V. On the application of mean-field and Landau theory to displacive phase transitions. *Ferroelectrics* **136,** 33–49 (1992).
10. Giddy, A. P., Dove, M. T., Pawley, G. S. & Heine, V. The determination of rigid unit modes as potential soft modes for displacive phase transitions in framework crystal structures. *Acta Crystallographica* **A49,** 697–703 (1993).
11. Perez-Mato, J. M., Withers, R. L., Larsson, A.–K., Orobengoa, D. & Liu, Y. Distortion modes and related ferroic properties of the stuffed tridymite-type compounds $SrAl_2O_4$ and $BaAl_2O_4$. *Phys. Rev. B* **79,** 064111 (2009).
12. Huang, S.-Y., Mühll, R. V. D., Ravez, J. & Couzi, M. Phase transition and symmetry in $BaAl_2O_4$. *Ferroelectrics* **159,** 127–132 (1994).
13. Huang, S.-Y. *et al.* A propos de la ferroélectricité dans $BaAl_2O_4$. *J. Solid State Chem.* **109,** 97–105 (1994).
14. Larsson, A.-K. *et al.* On the microstructure and symmetry of apparently hexagonal $BaAl_2O_4$. *J. Solid State Chem.* **181,** 1816–1823 (2008).
15. Avdeev, M., Yakovlev, S., Yaremchenko, A. A. & Kharton, V. V. Transitions between $P2_1$, $P6_3(\sqrt{3}A)$, and $P6_322$ modifications of $SrAl_2O_4$ by *in situ* high-temperature X-ray and neutron diffraction. *J. Solid State Chem.* **180,** 3535–3544 (2007).
16. Abakumov, A. M., Lebedev, O. I., Nistor, L., Tendeloo, G. V. & Amelinckx, S. The ferroelectric phase transition in tridymite type $BaAl_2O_4$ studied by electron microscopy. *Phase Trans*. **71,** 143–160 (2000).
17. Ishii, Y. *et al.* An unconventional phase transition in $BaAl_2O_4$ driven by two competing soft modes. arXiv:1510.02919 [cond-mat.mtrl-sci].
18. Stokes, H. T., Sadate, C., Hatch, D. M., Boyer, L. L. & Mehl, M. J. Analysis of the ferroelectric phase transition in $BaAl_2O_4$ by group theoretical methods and first-principles calculations. *Phys. Rev. B* **65,** 064105 (2002).
19. Rodehorst, U., Carpenter, M. A., Marion, S. & Henserson, C. M. B. Structural phase transitions and mixing behaviour of the Ba-aluminate ($BaAl_2O_4$)-Sr-aluminate ($SrAl_2O_4$) solid solution. *Mineral. Mag.* **67,** 989–1013 (2003).
20. Matsuno, K. *et al.* Charge ordering and spin frustration in $AlV_{2-x}Cr_xO_4$. *Phys. Rev. Lett.* **90,** 096404 (2003).
21. Horibe, Y. *et al.* Doping effect on the charge ordering in AlV_2O_4. *Phys. Rev. B* **71,** 052411 (2005).

22. Mori, S., Tokunaga, J., Horibe, Y., Aikawa, Y. & Katsufuji, T. Magnetocapacitance effect and related microstructure in Ti-doped $YMnO_3$. *Phys. Rev. B* **72,** 224434 (2005).
23. Weber, F. *et al.* Electron-phonon coupling and the soft phonon mode in $TiSe_2$. *Phys. Rev. Lett.* **107,** 266401 (2011).
24. Morosan, E. *et al.* Superconductivity in Cu_xTiSe_2. *Nature Phys*. **2,** 544–550 (2006).
25. Joe, Y. I. *et al.* Emergence of charge density wave domain walls above the superconducting dome in 1*T*-$TiSe_2$. *Nature Phys*. **10,** 421–425 (2014).
26. Yoshizawa, M. *et al.* Structural quantum criticality and superconductivity in iron-based superconductor $Ba(Fe_{1-x}Co_x)_2As_2$. *J. Phys. Soc. Jpn.* **81,** 024604 (2012).
27. Huang, S.-Y., Mühll, R. V. D., Ravez, J. & Hagenmuller, P. Structural, ferroelectric and pyroelectric properties of nonstoichiometric ceramics based on $BaAl_2O_4$. *J. Phys. Chem. Solids* **55,** 119–124 (1994).
28. Lemmens, H. *et al.* Transmission electron microscopy study of polymorphism in barium gallate $BaGa_2O_4$. *Phase Transitions* **76,** 653–670 (2003).

Acknowledgements

This work was partially supported by a Grant-in-Aid for Scientific Research from the Ministry of Education, Culture, Sports, Science and Technology of Japan (MEXT).

Author Contributions

Y.I. and S.M. conceived and designed the study. Y.I. and E.T. synthesized the materials. H.T. and S.M. conducted the TEM experiments. Y.I. analysed all of the data and wrote the paper. Y.I. and S.M. contributed to the discussion of the results.

Additional Information

Supplementary information accompanies this paper at http://www.nature.com/srep

Competing financial interests: The authors declare no competing financial interests.

How to cite this article: Ishii, Y. *et al.* A Fluctuating State in the Framework Compounds $(Ba,Sr)Al_2O_4$. *Sci. Rep.* **6**, 19154; doi: 10.1038/srep19154 (2016).